Performance comparison of different voltage control schemes on distributed generation

A. R. Di Fazio, G. Fusco, M. Russo

Faculty of Engineering, University of Cassino,
via G. Di Biasio 43, 03043 Cassino (FR), Italy.
russo@unicas.it

Abstract. The installation of Distributed Generation (DG) can have a significant impact on distribution system voltage regulation. The effects vary according to the DG device: in particular, synchronous generators present voltage control systems which interfere with the voltage regulation of the distribution systems. The paper analyzes two voltage control schemes for synchronous generators connected to MV distribution systems. They are designed according to different approaches: the first one is based on a fixed-parameter PID regulator whereas the second one employs an adaptive self-tuning technique. With reference to a case study, the two schemes are compared in terms of dynamic performance and dynamic interaction with distribution system voltage regulation, which is performed by the On-Load Tap Changer (OLTC) of the supplying HV/MV transformer.

Key words. Adaptive control, Distributed generation, Distribution systems, Synchronous generators, Voltage control.

1. Introduction

For many years, distribution systems were designed to deliver energy to the customers taking it from primary stations, without any generation in these systems. However, due to the recent changes of the legislative frame pushing towards liberalization of the electricity sector, generating units are being introduced into distribution systems. These generating units are referred to as Distributed Generation (DG).

The connection of DG close to the loads in distribution systems provides some benefits. It may increase power quality and reliability from the customers' perspective. It may also help the utilities to face the load growth by delaying the upgrade of distribution lines. Moreover, DG using renewable energies is often encouraged and financially supported thanks to its low environmental impact.

On the other hand, there are difficulties related to parallel operation of DG with the existing distribution systems [1]. In fact, the presence of DG introduces additional supplying nodes and may revert power flow directions along the feeders. The impact of DG on distribution system voltage profile is also significant [2]. Its effect varies according to the type of the DG device and depends on the distribution network characteristics. In particular, DG can be equipped with voltage control systems which interfere with voltage regulation of the distribution system.

The paper tackles the problem of comparing the performance achieved by two voltage control schemes on DG synchronous generators. The two schemes are designed according to different approaches: the first one is based on a fixed-parameter PID regulator whereas the second one employs an adaptive self-tuning technique. Particular attention is paid to dynamic performance and dynamic interaction with distribution system voltage regulation, which is performed by the On-Load Tap Changer (OLTC) of the supplying HV/MV transformer. The comparison refers to numerical simulations of a case study.

2. Distribution system voltage regulation

Improving nodal voltage profile in a MV distribution system is usually attained by changing the HV/MV substation transformer ratio using the OLTC and by connecting/disconnecting the capacitors in the substation and along the feeders of the distribution system. The voltage regulation problem in MV distribution system is traditionally split into two hierarchical levels: the off-line optimal setting problem and the on-line control problem.

The off-line problem determines, typically on a daily schedule, the optimal settings for the on-line voltage control reference signals and the optimal sequences of connection/disconnection of the capacitors.

The on-line problem aims at control of OLTC by closed loop regulation so as to keep the voltage amplitude close to the reference value $v_{\mathrm{T\,ref}}$ obtained from the off-line problem solution. In Figure 1 the voltage regulation scheme for OLTC is shown. The controlled voltage is either the measured transformer secondary voltage rms value $v_{\mathrm{T}}(t)$ or a calculated rms value $v_n(t)$ of the voltage of node n along the feeder. The latter case is usually referred to as Line Drop Compensation (LDC) principle. The LDC block in Figure 1 estimates $v_n(t)$ from the measurements of the apparent power $p_{\mathrm{T}}(t) + jq_{\mathrm{T}}(t)$ supplied by the transformer to the distribution system, according to:

$$v_n(t) = v_{\mathrm{T}}(t) + \mathrm{r_c}\frac{p_{\mathrm{T}}(t)}{v_{\mathrm{T}}(t)} + \mathrm{x_c}\frac{q_{\mathrm{T}}(t)}{v_{\mathrm{T}}(t)}, \qquad (1)$$

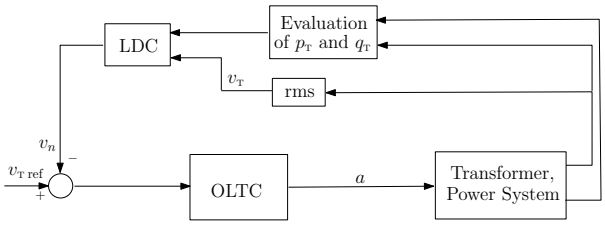

Fig. 1. Voltage regulation scheme for OLTC.

where $\mathrm{r_c}$ and $\mathrm{x_c}$ are, respectively, the resistance and the inductance to be compensated, that is the resistance and inductance of the line between the transformer and the node n along the feeder.

The aim of the regulation is to guarantee that the error between the controlled voltage $v_n(t)$ and the voltage reference $v_{\rm T\,ref}(t)$ is kept inside an accepted range of tolerance, despite the presence on disturbances. For this purpose, the OLTC varies the transformer ratio a. For a detailed description of the features of the voltage regulation performed by the OLTC refer to [3].

3. Voltage control schemes on distributed synchronous generators

The performance of the on-line voltage regulation may be strongly affected by DG connected to the distribution system. In some cases, the presence of DG may cause over-voltages by injecting active power along the feeders; in other cases, when LDC is adopted, DG may cause under-voltages because its presence reduces the current supplied by the transformer and, consequently, the OLTC compensation.

The interaction between the distribution system voltage regulation and the DG varies significantly according to the type of electrical interfaces between DG and the distribution system. In particular, DG adopting synchronous generators is usually equipped with voltage control systems. Then, the dynamic interaction between the DG devices and the OLTC voltage regulation must be analyzed.

The design of two different control schemes are presented.

The first one is a fixed-parameter Automatic Voltage Regulator (AVR), often adopting a PID structure. Such scheme may be enriched with additional VAR/power-factor external control loops, see [4].

The second voltage control scheme is based on the use of adaptive self-tuning technique. It is derived from the general scheme proposed in [5] for the specific case of synchronous generators. It uses a frequency domain model based on the Thevenin equivalent circuit, which models power system response to changes of the synchronous generator operating point.

The phasor equation associated with the Thevenin equivalent circuit shown in Figure 2 is

$$\bar{v}_{\rm G}(t) = \bar{v}_0(t) + \bar{\mathrm{z}}_{\rm eq}\,\bar{\imath}_{\rm G}(t) \qquad (2)$$

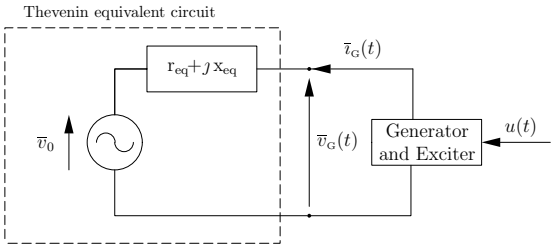

Fig. 2. Phasor representation of the power system using the Thevenin equivalent circuit.

where

$$\begin{aligned} \bar{\mathrm{z}}_{\rm eq} &= \mathrm{r_{eq}} + \jmath\,\mathrm{x_{eq}} \\ \bar{v}_0(t) &= v_{0,r}(t) + \jmath\, v_{0,i}(t)\,. \end{aligned}$$

Concerning the synchronous generator, in the framework of voltage amplitude control problem, the following simplifications are typically assumed [6] by neglecting

- the stator "transformer emfs", that is the emfs due to magnetic flux time derivatives,
- the effects of speed variation on stator voltage,
- the distortion of stator voltage and current waveforms.

The transformer emfs can be neglected because the electrical transients associated with them rapidly decay compared to the transients involved in voltage control. The second assumption generally counterbalances the approximations introduced by the former one. The third assumption is very close to reality, especially for large-sized generators. With such assumptions, it is possible to adopt a model that uses time-varying phasors at fundamental frequency to represent stator voltages and currents.

The synchronous generator phasor model is described by adopting the Park transformation changing the three-phase phasors to the $(d-q-0)$ representation. The $(d-q)$ axes are fixed to the rotor flux magnetic axis. Concerning the 0 axis, which is fixed in space, since the zero-sequence component of the stator current is usually null, in the above assumptions no voltage is present. The synchronous generator stator voltage $\bar{v}_{\rm G}(t)$ and current $\bar{\imath}_{\rm G}(t)$ phasors are represented, respectively, as

$$\bar{v}_{\rm G}(t) = v_{{\rm G},d}(t) + \jmath\, v_{{\rm G},q}(t) \qquad (3)$$

$$\bar{\imath}_{\rm G}(t) = \imath_{{\rm G},d}(t) + \jmath\, \imath_{{\rm G},q}(t) \qquad (4)$$

while the stator voltage amplitude is

$$v_{\rm G}(t) = |\bar{v}_{\rm G}(t)| = \sqrt{v_{{\rm G},d}^2(t) + v_{{\rm G},q}^2(t)}\,. \qquad (5)$$

According to the above assumptions, and neglecting the nonlinear effect of saturations, the following simplified transfer functions can be adopted to model the synchronous generator in the Laplace operator s [7]

$$V_{{\rm G},d}(s) = \mathrm{x}_{{\rm G},q}(s)\, I_{{\rm G},q}(s) \qquad (6)$$

$$V_{{\rm G},q}(s) = \mathrm{a}_{\rm G}(s)\, V_{ex}(s) - \mathrm{x}_{{\rm G},d}(s)\, I_{{\rm G},d}(s) \qquad (7)$$

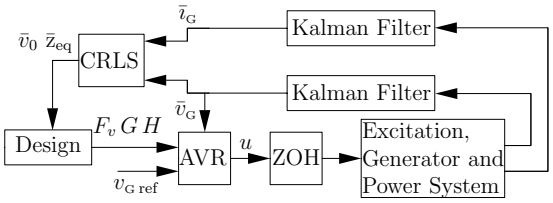

Fig. 3. Adaptive nodal voltage control scheme.

where $\mathrm{x}_{\mathrm{G},d}(s)$ and $\mathrm{x}_{\mathrm{G},q}(s)$ are operational transfer functions modeling the generator reactance (sub-transient, transient and synchronous) along, respectively, d and q axis. The input is $V_{ex}(s)$, that is the $\mathcal{L}$-transform of the rotor excitation voltage as seen from the stator windings, namely $v_{ex}(t)$. Then, in (7) $\mathrm{a}_{\mathrm{G}}(s)$ represents the stator voltage transfer function in no-load operating conditions, that is with null stator current.

In addition to (6)-(7), it is necessary to model also the dynamic response of the exciter to represent the actual variation of $v_{ex}(t)$ in response to a variation of the command input $u(t)$. Such a response is strictly dependent on the exciter characteristics. Among different types of exciter configuration that can be used [8], in the remainder we will refer to a rectifier-based excitation system.

To model the dynamic response of the exciter, the thyristor bridge rectifier can be represented by including a time delay τ_{ex}, which is obviously set equal to $1/6$ of the time period of the fundamental frequency, and a time constant T_{ex}, which is equal to $3-4$ ms, yielding the following transfer function:

$$\mathrm{E}(s) = \frac{V_{ex}(s)}{U(s)} = \frac{e^{\,s\,\tau_{ex}}}{1 + s\,T_{ex}}. \tag{8}$$

The structure of the proposed adaptive AVR control scheme is shown in Fig. 3. The two blocks named Kalman Filters are necessary to identify and track the values of the voltage and current phasors at fundamental frequency at the regulation node, namely $\bar{v}_{\mathrm{G}}$ and $\bar{\imath}_{\mathrm{G}}$. These values are the inputs of the block named CRLS in which the parameters of the Thevenin equivalent circuit are estimated every T_e seconds using a constrained recursive least-squares algorithm. The estimated parameters are subsequently sent to the block denoted as Design to determine, according to well-established discrete-time design techniques, the polynomials F_v, G and H. Such polynomials concur to define the control input u which is calculated in the block named AVR.

To estimate the parameters r_{eq}, x_{eq}, $v_{0,r}$ and $v_{0,i}$ let us considering model (2) written including dynamics only on current phasors (first order model). Accordingly one has

$$\mathbf{y}(t_{e,k}) = \begin{bmatrix} v_r(t_{e,k}) & v_i(t_{e,k}) \end{bmatrix} = \boldsymbol{\psi}(t_{e,k})\,\boldsymbol{\Theta} \tag{9}$$

in which $\boldsymbol{\Theta} \in \mathbb{R}^{5\times 2}$, where $t_{e,k} = k\,T_e$ denotes the kth time sample with $k \in \boldsymbol{Z}$ and

$$\begin{aligned} \boldsymbol{\psi}(t_{e,k}) \;=\; & \Big[\imath_{\mathrm{G},r}(t_{e,k}) \qquad \imath_{\mathrm{G},i}(t_{e,k}) \qquad c_v \\ & \qquad \imath_{\mathrm{G},r}(t_{e,k-1}) \qquad \imath_{\mathrm{G},i}(t_{e,k-1})\Big]. \end{aligned} \tag{10}$$

In (10) the quantity c_v is a constant input; it acts as a scaling factor.

Since in steady-state it is

$$\begin{aligned} \imath_{\mathrm{G},r}(t_{e,k}) &= \imath_{\mathrm{G},r}(t_{e,k-1}) = \imath_{\mathrm{G},r}(\infty) \\ \imath_{\mathrm{G},i}(t_{e,k}) &= \imath_{\mathrm{G},i}(t_{e,k-1}) = \imath_{\mathrm{G},i}(\infty) \end{aligned}$$

the steady-state value $\boldsymbol{y}(\infty)$ of the output model (9) is given by

$$\mathbf{y}(\infty) = \begin{bmatrix} \imath_{\mathrm{G},r}(\infty) & \imath_{\mathrm{G},i}(\infty) & c_v \end{bmatrix} \begin{bmatrix} \theta_{11}+\theta_{41} & \theta_{12}+\theta_{42} \\ \theta_{21}+\theta_{51} & \theta_{22}+\theta_{52} \\ \theta_{31} & \theta_{32} \end{bmatrix}. \tag{11}$$

Comparing (2) with (11), it is possible to derive the following "physical" conditions on the parameters

$$\begin{bmatrix} \theta_{11}+\theta_{41} & \theta_{12}+\theta_{42} \\ \theta_{21}+\theta_{51} & \theta_{22}+\theta_{52} \\ \theta_{31} & \theta_{32} \end{bmatrix} = \begin{bmatrix} \mathrm{r}_{\mathrm{eq}} & \mathrm{x}_{\mathrm{eq}} \\ -\mathrm{x}_{\mathrm{eq}} & \mathrm{r}_{\mathrm{eq}} \\ \dfrac{v_{0,r}}{c_v} & \dfrac{v_{0,i}}{c_v} \end{bmatrix}. \tag{12}$$

To estimate matrix $\boldsymbol{\Theta}$, the following prediction model of the output variable $\widehat{\mathbf{y}}(t_{e,k})$ is considered:

$$\widehat{\mathbf{y}}(t_{e,k}) = \boldsymbol{\psi}_h(t_{e,k})\,\widehat{\boldsymbol{\Theta}}(t_{e,k-1}).$$

Applying a recursive least-squares algorithm constrained by (12), it is possible to obtain $\widehat{\boldsymbol{\Theta}}$ which enables to determine the parameters r_{eq}, x_{eq}, $v_{0,r}$ and $v_{0,i}$ according to [5]

$$\begin{aligned} \widehat{\mathrm{r}}_{\mathrm{eq}} &= \boldsymbol{w}_1^{\mathrm{T}}\widehat{\boldsymbol{\Theta}}_1 \\ \widehat{\mathrm{x}}_{\mathrm{eq}} &= \boldsymbol{w}_1^{\mathrm{T}}\widehat{\boldsymbol{\Theta}}_2 \\ \widehat{v}_{0,r} &= c_v\,\hat{\theta}_{31} \\ \widehat{v}_{0,i} &= c_v\,\hat{\theta}_{32} \end{aligned}$$

in which

$$\begin{aligned} \boldsymbol{w}_1 &= \begin{bmatrix} 1 & 0 & 0 & 1 & 0 \end{bmatrix}^{\mathrm{T}} \\ \boldsymbol{w}_2 &= \begin{bmatrix} 0 & 1 & 0 & 0 & 1 \end{bmatrix}^{\mathrm{T}}. \end{aligned}$$

Concerning the structure of the AVR, it is sketched in Figure 4. The polynomials

$$\begin{aligned} F_v(z^{-1}) &= 1 + f_{v,1}z^{-1} + \ldots + f_{v,n_{F_v}}\,z^{-n_{F_v}} \\ G(z^{-1}) &= g_0 + g_1 z^{-1} + \ldots + g_{n_G}\,z^{-n_G} \\ H(z^{-1}) &= h_0 + h_1 z^{-1} + \ldots + h_{n_H}\,z^{-n_H} \end{aligned}$$

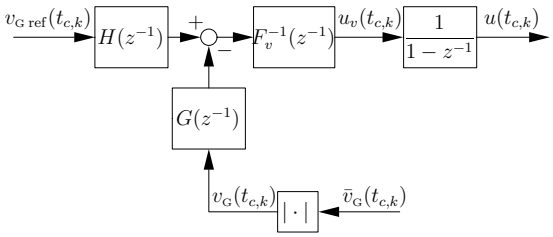

Fig. 4. AVR block scheme.

in the backward shift operator z^{-1} define the regulator law

$$(1-z^{-1})\,F_v(z^{-1})\,u(t_{c,k}) = -\,G(z^{-1})\,v_{\mathrm{G}}(t_{c,k}) + H(z^{-1})\,v_{\mathrm{G\,ref}}(t_{c,k}) \quad (13)$$

where $t_{c,k} = kT_c$ being T_c the sampling period.

In the block named Design in Figure 3, the polynomials $F_v(z^{-1})$, $G(z^{-1})$ and $H(z^{-1})$ are designed on the basis of the pole-assignment technique [9]. To this aim let us consider the following transfer function

$$M(z^{-1}) = \left(\frac{1}{1-z^{-1}}\right)\mathcal{Z}\Big\{ZOH(s)\,R(s)\Big\} = \mathcal{Z}\Big\{\frac{R(s)}{s}\Big\} = z^{-d}\,\frac{B^{+}(z^{-1})\,B^{-}(z^{-1})}{A(z^{-1})} \quad (14)$$

describing the relationship between the control input $u_v(t_{c,k})$ and the stator voltage amplitude $v_{\mathrm{G}}(t_{c,k})$ and where polynomials $B^{+}(z^{-1})$ and $B^{-}(z^{-1})$ have their roots inside and outside the unit circle, respectively. Moreover, in (14) the term z^{-d} appears since model (8) includes a pure time delay τ_{ex} which is not, in practice, an exact multiple of the sampling period T_c. However, this time delay can be expressed as

$$\tau_{ex} = d\,T_c - \rho\,T_c$$

with d a positive integer and $0 \le \rho \le 1$. The transfer function $R(s)$ it is given by

$$R(s) = \frac{\Delta V_{\mathrm{G}}(s)}{\Delta V_{ex}(s)}\,\mathrm{E}(s)$$

in which

$$\frac{\Delta V_{\mathrm{G}}(s)}{\Delta V_{ex}(s)} = \widehat{\mathrm{z}}_{\mathrm{eq}}^{2}\left(\left(\frac{v_{\mathrm{G},d}^{*}}{v_{\mathrm{G}}^{*}}\,\widehat{\mathrm{r}}_{\mathrm{eq}} + \frac{v_{\mathrm{G},q}^{*}}{v_{\mathrm{G}}^{*}}\,\widehat{\mathrm{x}}_{\mathrm{eq}}\right)\mathrm{x}_{\mathrm{G},q}(s) + \frac{v_{\mathrm{G},q}^{*}}{v_{\mathrm{G}}^{*}}\,\widehat{\mathrm{z}}_{\mathrm{eq}}^{2}\right)\frac{\mathrm{a}_{\mathrm{G}}(s)}{\mathrm{w}(s)}, \quad (15)$$

where

$$\mathrm{w}(s) = \widehat{\mathrm{r}}_{\mathrm{eq}}^{2}\,\mathrm{x}_{\mathrm{G},d}(s)\,\mathrm{x}_{\mathrm{G},q}(s) + \Big(\widehat{\mathrm{z}}_{\mathrm{eq}}^{2} + \widehat{\mathrm{x}}_{\mathrm{eq}}\,\mathrm{x}_{\mathrm{G},q}(s)\Big)\Big(\widehat{\mathrm{z}}_{\mathrm{eq}}^{2} + \widehat{\mathrm{x}}_{\mathrm{eq}}\,\mathrm{x}_{\mathrm{G},d}(s)\Big).$$

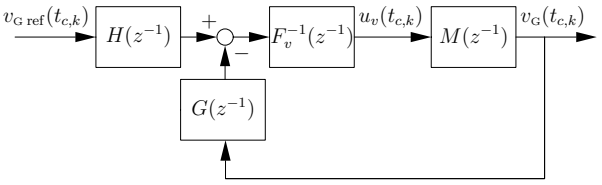

Fig. 5. Closed-loop equivalent system.

In (15) Δ symbol denotes variations with respect to steady-state values represented by starred quantities.

The concluding design step consists of determining the coefficients of the polynomials $F_v(z^{-1})$, $G(z^{-1})$ and $H(z^{-1})$. To this aim it is useful to remind that the regulator cancels the zeros of $B^{+}(z^{-1})$. For this reason $F_v(z^{-1})$ is factorized as

$$F_v(z^{-1}) = B^{+}(z^{-1})\,\widetilde{F}(z^{-1}). \quad (16)$$

Polynomials $\widetilde{F}(z^{-1})$ and $G(z^{-1})$ are designed according to the pole assignment technique. To this aim, a polynomial $T(z^{-1})$ is assigned, whose roots represent the desired closed loop poles. Then, $\widetilde{F}(z^{-1})$ and $G(z^{-1})$ are obtained by solving every ℓ steps, with ℓ a fixed integer, the following Diophantine equation

$$A(z^{-1})\,\widetilde{F}(z^{-1}) + z^{-d}\,B^{-}(z^{-1})\,G(z^{-1}) = T(z^{-1}) \quad (17)$$

which has an unique solution if $A(z^{-1})$ and $B(z^{-1})$ are co-prime and following constraints

$$n_{\widetilde{F}} = d - 1 + n_{B^{-}} \quad (18)$$

$$n_{G} = n_{A} - 1 \quad (19)$$

$$n_{T} = n_{A} + n_{B^{-}} + d - 1 \quad (20)$$

are fulfilled. From solution of Diophantine equation (17) one obtains $F_v(z^{-1})$ from (16) while the simplest choice for $H(z^{-1})$ leads to

$$H(z^{-1}) = h_0 = \left.\frac{T(z^{-1})}{B^{-1}(z^{-1})}\right|_{z^{-1}=1}.$$

The block scheme of the closed loop equivalent system is reported in Figure 5.

4. Case study

To compare the two voltage control schemes applied to the DG in terms of both their performance and their effects on the distribution system voltage regulation a case study has been considered.

The simple distribution system shown in Fig. 6 presents a 20 kV feeder, supplied from a HV/MV trasformer equipped with OLTC, and a DG device, that can be connected to any load busbar. The network data are reported in Table I.

The DG device is assumed to be equipped with a controlled synchronous generator, whereas the prime mover

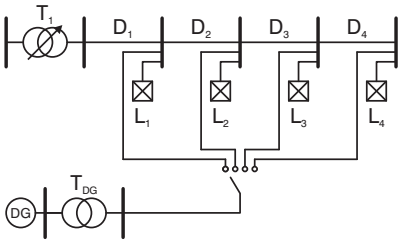

Fig. 6. Test distribution system.

TABLE I
NETWORK DATA

LINES			LOADS		
	R [Ω]	X [Ω]		P [kW]	Q [kVAr]
D_1	0.6843	0.9612	L_1	626	306
D_2	0.6843	0.9612	L_2	545	266.7
D_3	0.4562	0.6408	L_3	2737	1388
D_4	0.2281	0.3204	L_4	4916	2403.7

TABLE II
DG DEVICE DATA

DISPERSED GENERATOR					
Rotor type	P_n [MVA]	V_n [Vrms]	f_n [Hz]	R_s [p.u.]	Time constants
Salient pole	2	380	50	0.003	Short circuit
X_d [p.u.]	X'_d [p.u.]	X''_d [p.u.]	X_q [p.u.]	X''_q [p.u.]	X_l [p.u.]
3.28	0.322	0.161	1.88	0.181	0.04
T'_d [s]	T''_d [s]	T''_q [s]	H [s]	F [p.u.]	p [.]
0.35	0.0036	0.0036	2	0.01	2

DG TRANSFORMER				
Type of winding	P_n [MVA]	V_1 [Vrms]	V_2 [Vrms]	R_1 [p.u.]
YgY	2.5	380	20000	0.00398
L_1 [p.u.]	R_2 [p.u.]	L_2 [p.u.]	R_m [p.u.]	L_m [p.u.]
0.0398	0.00398	0.0398	500	500

TABLE III
HV/MV STATION DATA

TRANSFORMER T_1 WITH OLTC				
Type of winding	P_n [MVA]	$v_{T\,ref}$ [p.u.]	a_{min} ratio	a_{max} ratio
YgY	12	0.97	0.85	1.05
R_{T1} [p.u.]	X_{T1} [p.u.]	R_{T2} [p.u.]	X_{T2} [p.u.]	n_{pos} [.]
0.00398	0.0398	0.00398	0.0398	21

generates an assigned mechanical power (1.6 MW) and no speed governor is present. The data related to the DG synchronous generator and transformer are reported in Table II, whereas Table III is referred to HV/MV transformer data. The p.u. quantities are calculated assuming as reference basis the rated power of each device and the 20 kV system rated voltage.

In the following CASE A refers to DG equipped with a classical PI regulator, whereas CASE B to the adaptive control scheme recalled in Sect. 3. The comparison is performed in the case of DG connected at busbar with load L_1. In fact, this is the case in which the DG is electrically nearest to the substation transformer and, consequently, there is the strongest possible coupling between the control systems respectively of the OLTC and of the DG. Concerning the OLTC, it adopts a simple integrator with a deadband and LDC is performed to obtain the voltage v_3 at the busbar with load L_3.

The simulations have been performed in Matlab/Power System Blockset environment. Respectively for CASE A and CASE B, Figures 7 and 8 show the time evolutions of the voltage v_T at the MV busbar of the primary supplying station, of the voltage v_G at the synchronous generator terminals and of the voltage v_3 at the compensated node of the distribution feeder.

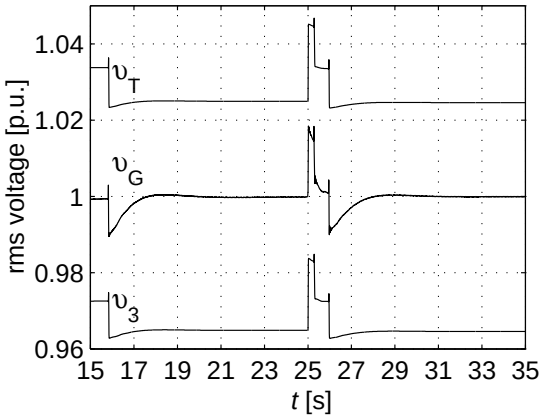

Fig. 7. CASE A: Time evolution of voltages v_T, v_G and v_3

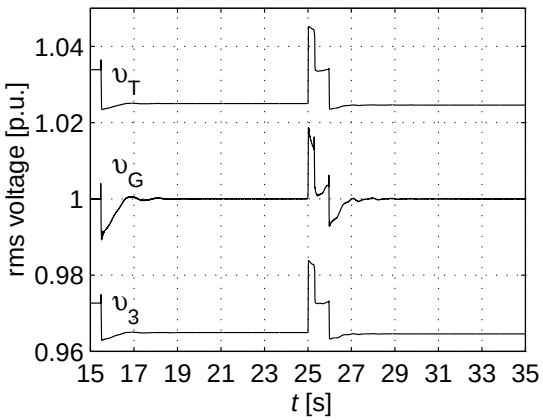

Fig. 8. CASE B: Time evolution of voltages v_T, v_G and v_3

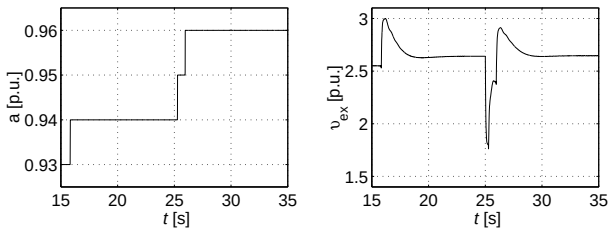

Fig. 9. CASE A: Time evolution of commands a and v_{ex}

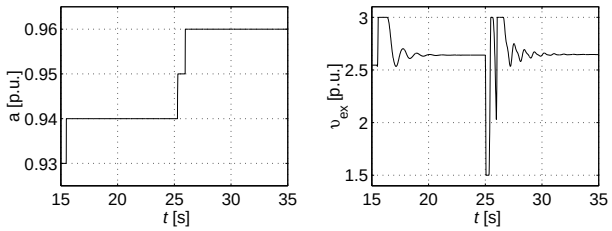

Fig. 10. CASE B: Time evolution of commands a and v_{ex}

Concerning the commands, Figures 9 and 10 report the time evolutions of the ratio a of the HV/MV transformer and of the excitation voltage v_{ex} of the DG, respectively for CASE A and CASE B. The considered time interval starts from time instant equal to 15 s, that is only after that the steady-state operating conditions have been reached.

At time instant equal to 15 s a step variation is applied to $v_{\mathrm{T\,ref}}$, which changes from 0.97 to 0.96 p.u.. Analyzing Figures 9 and 10, it is apparent that there is a delay in the change of the HV/MV transformer ratio a due to the deadband in the OLTC regulator. Consequently, the DG voltage control reacts to the variation of v_{G} by changing the excitation voltage v_{ex}. Comparing the time evolutions of voltages (Figures 7 and 8), the response assured by the adaptive control scheme (CASE B) is faster than the one obtained in CASE A.

At time instant equal to 25 s a step variation is applied to the no-load voltage at the HV busbar of the primary supplying station, which changes from 1.0 to 1.02 p.u.. Due to the change of the system operating conditions, both OLTC regulator and DG voltage control react to the voltage perturbation. In particular (Figures 9 and 10) two changes of the HV/MV transformer ratio a take place: the first one after about 0.1 s and the second one after about 1 s. The time evolution of voltages (Figures 7 and 8) show the strong interaction between the synchronous voltage control action and the OLTC regulation. It is important to notice that, due to the different operating conditions, the standard PI control scheme presents a larger rising time with respect to the one assured in the previous perturbation. On the contrary, the adaptive control scheme guarantees always the same rising time and, consequently, the responses of the voltages after OLTC step variations are much faster with respect to the performance obtained by the standard PI controller. Such higher performance is obtained by the adaptive control scheme thanks to a stronger action on the excitation

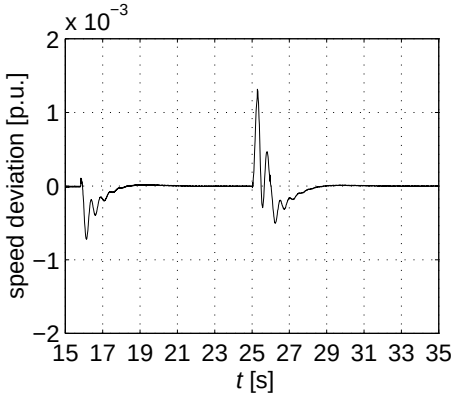

Fig. 11. CASE A: Time evolution of DG rotor speed deviation

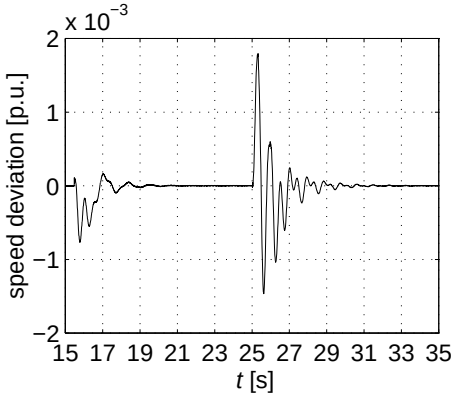

Fig. 12. CASE B: Time evolution of DG rotor speed deviation

system, as clearly shown in Figures 9 and 10. Eventually, the larger and faster variations of the excitation voltage required by the adaptive control scheme increases the mechanical oscillations of the synchronous generator. Figures 11 and 12 show the rotor speed deviation, respectively for CASE A and CASE B. It is apparent that in CASE B the mechanical oscillation amplitudes, although still quite limited, are larger that the ones obtained in CASE A.

5. Conclusions

The paper analyzes two voltage control schemes for distributed synchronous generators connected to MV distribution systems. The schemes are designed according to two different approaches: the first one is based on a fixed-parameter PID regulator whereas the second one employs an adaptive self-tuning technique. With reference to a case study, the two schemes are compared in terms of dynamic performance and dynamic interaction with distribution system voltage regulation, which is performed by the On-Load Tap Changer (OLTC) of the supplying HV/MV transformer. The simulation results have shown that the adaptive control scheme assures a faster voltage recovery in response to variations of the system operating conditions. However, such higher performance requires a more intensive control action on the DG. Further studies will investigate the possibility

of adopting innovative control techniques also on the OLTC and of improving the coordination between the DG voltage control schemes and the distribution system voltage regulation.

References

[1] CIGRÉ Working Group 37-23, "Impact of increasing contribution of dispersed generation on the power system," *CIGRÉ Final Report*, vol. 137, Feb. 1999.

[2] A. Losi and M. Russo, "Dispersed generation modeling for object oriented distribution load flow," *IEEE Trans. on Power Delivery*, vol. 20, no. 2, pp. 1532–1540, Apr. 2005.

[3] G. M. Casolino, A. Losi, and M. Russo, "Modeling voltage regulation in object-oriented analysis of distribution systems including dispersed generation," in *IFAC Symposium on Power Systems & Power Plants*, vol. PN 527, Kananaskis, Canada, Jun. 2006.

[4] T. W. Eberly and R. C. Schaefer, "Voltage versus var/power-factor regulation on synchronous generators," *IEEE Trans. on Industry Applications*, vol. 38, no. 6, pp. 1682–1687, Nov./Dec. 2002.

[5] G. Fusco and M. Russo, "Self-tuning regulator design for nodal voltage waveform control in electrical power systems," *IEEE Trans. on Control Systems Technology*, vol. 11, no. 2, pp. 258–266, Mar. 2003.

[6] P. Kundur, *Power System Stability and Control*. New York, USA: Mc-Graw Hill, Inc, 1994.

[7] R. Marconato, *Electric Power System: Background and Basic Concepts*, 2nd ed. Milano, Italy: CEI Italian Electrotechnical Committee, 2002, vol. 1.

[8] *IEEE Recommended Practice for Excitation System Models for Power System Stability Studies*, IEEE Std. 421.5, 2005.

[9] P. Wellstead and M. Zarrop, *Self-tuning System Control and Signal Processing*. New York, USA: John Wiley & Sons, 1991.